Int. J. Heat Mass Transfer. Vol. 25, No. 10, pp. 1579–1588, 1982
Printed in Great Britain

0017–9310/82/101579–10 $03.00/0
Pergamon Press Ltd.

LOCAL VELOCITY AND MASS TRANSFER MEASUREMENTS IN MOLTEN METALS USING AN INCORPORATED MAGNET PROBE

RENE RICOU and CHARLES VIVES

Laboratoire de Magnétohydrodynamique, Faculté des Sciences,
33, rue Louis Pasteur, 84000 Avignon, France

(*Received* 10 *November* 1981 *and in revised form* 8 *March* 1982)

Abstract—A probe permitting the determination of the velocity magnitude and direction at every point for a steady or time-varying state within a molten metal is described. Understanding the working principle of this sensor is founded on an experimental study of the flow of a liquid metal around a cylindrical magnet. Examples of velocity distributions plotted from room temperature (mercury) up to 670°C (aluminium alloys) within flows containing vortices are presented. Results indicate that local velocities within the range 0–10 m s^{-1}, with a sensitivity of the order of 1 mm s^{-1}, can be measured in baths with temperatures as high as 720°C.

NOMENCLATURE

η, viscosity;
ρ, density;
ν, kinematic viscosity;
σ, electrical conductivity of liquid metal;
σ', electrical conductivity of the cylindrical obstacle;
σ^*, σ/σ';
B_0, magnetic field of external origin;
B, local value of the magnetic field;
B_r, B_z, radial and axial components of B;
H_c, coercive force;
E, electric field;
J, current density;
V, voltage;
$V_{AA'}, V_{BB'}$, voltage between electrodes A and A', and B and B';
d, diameter of the cylindrical obstacle (or probe);
D, distance between electrodes AA' (or BB');
l, height of the obstacle (or of the probe);
L, width of the square cross-section duct;
R_1, R_2, annular vessel radii;
h, annular vessel depth;
ΔP, pressure difference;
F, pressure resultant force upon the cylinder (calculated by unit length);
U, average velocity;
u, local velocity;
u_x, u_y, u_z, components of u;
a, magnitude of the alternating motion;
ω, angular velocity;
U_m, maximal value of the velocity in alternating state;
U', RMS velocity;
r, θ, z, cylindrical polar coordinates;
r, θ, ϕ, spherical coordinates;
T, temperature;
K, calibration factor of the probe;
Re, Reynolds number of the cylinder (or of the probe), $(Ud)/\nu$;
Re', Reynolds number of the duct, $(UL)/\nu$;
M, Hartmann number of the cylinder (or of the probe), $Bd(\sigma/\eta)^{1/2}$;
N, Stuart number (interaction parameter) of the cylinder, M^2/Re; (or of the probe)
C_p, pressure drag of the cylindrical obstacle, $2F/(\rho U^2 d)$.

1. INTRODUCTION

MEASUREMENT methods of classical fluid mechanics are ineffectual when it comes to measuring local velocities in steady or unsteady states within molten metals of high melting point. The use of flow visualization methods (interferometers) is excluded on account of the opacity of these liquids. Various sensors, such as the Pitot–Prandtl tubes [1], with a working principle founded on pressure difference measurements, are ineffective due to metal solidification within the manometric tubes. Hot-wire and hot-film sensors permit plotting of the average value of velocities as well as pulsatile velocities inside mercury flows [2–8]. However, the high thermal conductivity of the liquid metal plus the necessity of keeping a very nearly constant temperature make the use of the probes especially difficult. In addition, hot-wire and hot-film techniques do not seem to have been employed with temperatures in excess of 100°C [6].

The importance of further studying convection phenomena and mass transfer inside fusion reactors using molten metals as coolant fluids, plus the value of a better understanding of local velocities and flow rates during casting in metallurgy, have led us to perfect a new measurement method [9] based upon the fundamental study of a liquid metal flow around a permanent magnet of cylindrical shape.

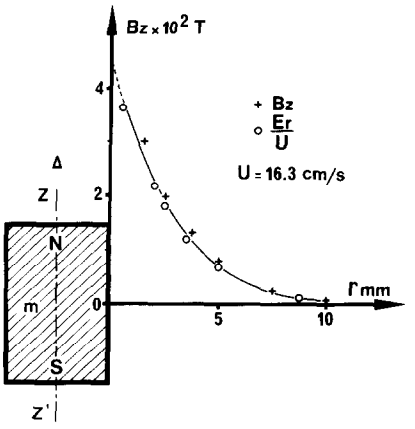

FIG. 1. Distribution of the axial component B_z of the magnetic field.

2. FUNDAMENTAL ASPECTS

The complexity of theory dealing with flow states of a viscous and conducting liquid around a magnetic cylinder of finite length which provides a non-uniform magnetic field in a local vicinity led us to a methodical and exclusively experimental study. This study was conducted upon a number of magnets with diameters ranging from 2 to 30 mm and fabricated from Alnico, ferrites, or cobalt–rare-earth.

2.1. *Pattern of the magnetic field*

The components of the magnetic field were locally measured at room temperature with a small Hall-effect probe, the sensitive element dimensions of which were 2 × 2 × 0.5 mm. Figure 1 presents a measurement example using a cylindrical permanent magnet (Coramag) with a Δ revolution axis, a diameter d of 4.95 mm, and a length l of 7.5 mm. It was found that the axial components B_z, parallel to the Δ-axis and plotted at the midpoint of the height of the magnet along a radial axis $\vec{0r}$, decreased very rapidly. Thus B_z varies to 0.044 T when $r = 0$ (value upon the magnet wall, obtained by extrapolation) from 10^{-3} T, when $r = 2d$ (Fig. 1). Measurements also showed that radial components B_r of the magnetic field, once again plotted at midheight along the y-axis, are practically negligible.

2.2. *Pressure distribution on the cylinder*

2.2.1. *Summary of earlier studies.* Earlier experimental work [10–13] describes magnetohydrodynamic flows around cylindrical, insulating or conducting obstacles, having generators perpendicular to the mean direction of flow of a liquid metal of density ρ, kinematic and dynamic viscosities ν and η, and electric conductivity σ. A solid cylinder of diameter d was placed at the center of a square cross-section duct made from an insulating material (Plexiglas) and in which mercury was allowed to flow. Both a pressure tap of variable azimuth θ (with respect to the direction of the average velocity **U**), situated at midheight upon the cylinder, and a second pressure tap situated upstream at point 0 of a wall of the duct, were connected to an electromagnetic manometer [14]. This device allowed the plotting of pressure difference profiles $\Delta P_{(\theta)} = P_\theta - P_0$ as a function of θ for different values of the Reynolds number $Re = Ud/\nu$ and of the Hartmann number $M = B_0 d(\sigma/\eta)^{1/2}$ relative to the obstacle.

It is important to remember that in classical fluid mechanics, pressure drop profiles are only known to a nearest constant, corresponding to a hydrodynamic duct loss which depends upon the position of the pressure tap P_0 (Fig. 2b). In magnetofluidmechanics, another pressure difference occurs on account of an electromagnetic pressure gradient inside the duct. This second pressure drop is a function of M, of Re, of the magnetical and mechanical boundary conditions, and, once again, of the position of P_0.

Our results reflected the fact that if a uniform and stationary magnetic field $\mathbf{B}_0$ is perpendicularly applied both to **U** and the Δ-axis, the function $\Delta P_{(\theta)}$ plotted for constant Reynolds numbers is considerably modified, as well as the pressure drag coefficient

$$C_p = 2F/\rho U^2 d,$$

with

$$F = \int_0^\pi \Delta P_{(\theta)} \cdot d \cdot \cos\theta \cdot d\theta$$

calculated by unit length of the cylinder.

These effects, which depend upon the Reynolds number Re, the Hartmann number M, the Stuart number N (interaction parameter), as well as the ratio $\sigma^* = \sigma/\sigma'$ of the electric conductivity of the liquid σ and the cylinder σ', were explained by the appearance of a supplementary pressure of electromagnetic origin coming from the interaction between $\mathbf{B}_0$ and the very high eddy current densities **J** which existed in the boundary layer surrounding the obstacle.

On the other hand, if $\mathbf{B}_0$ was parallel to the Δ axis [11], the shape of the pressure drop profiles, and the pressure drag coefficients as well, were practically independent from the values of M and σ^* for a given Re. Hence it can be assumed that, in this particular situation, there was no important magnetohydrodynamic effect in the boundary layer, and the boundary layer remained unchanged. The induced electrical currents circulating in the nearest vicinity of the obstacle were consequently at a zero value, or very weak.

2.2.2. *Ferromagnetic cylinders.* Two honeycombs were fitted upstream and downstream with respect to the cylinder so as to smooth out non-uniformities in the velocity profile coming from fringe phenomena of hydrodynamic and magnetohydrodynamic origin [1, 15]. Upon experimentation, the Reynolds number, $Re' = (UL)/\nu$, of a duct of width $L = 68$ mm was constantly in excess of 4000 and subsidiary measurements verified that the uniformity of the velocity profile was quite nearly realized (U = constant in a cross-section upstream from the obstacle).

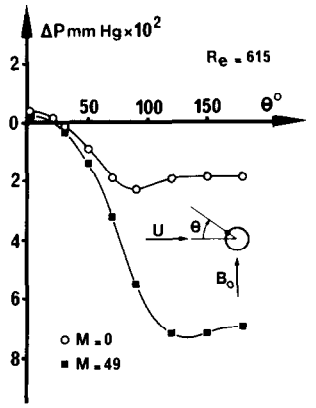

FIG. 2(a). Pressure profiles around a cylinder of soft iron subjected to a transverse magnetic field as a function of angle θ.

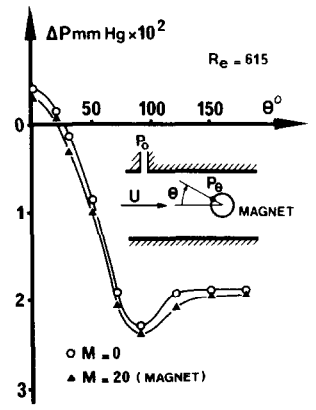

FIG. 2(b). Pressure profiles around a cylindrical permanent magnet as a function of angle θ.

Figure 2(a) shows pressure profiles arising from a ferromagnetic cylinder of 1 cm dia. and 2 cm height made from soft iron. An electromagnet produces a stationary magnetic field which, in the absence of an obstacle, is practically uniform and perpendicular both to **U** and to the Δ-axis [13]. The value of the magnetic field **B** chosen to determine the Hartmann number is the same which exists, for the same magnetic intensity, in the presence of a non-magnetic cylinder (or in the absence of an obstacle). The pressure difference was found to vary considerably with M. This pronounced effect can be explained once again by the existence of a magnetohydrodynamic boundary layer where an electric field **E** and an induced current density **J** are strongly concentrated.

Next we experimented with a permanent magnet of dimensions identical to the soft iron cylinder (d = 1 cm, l = 2 cm). For calculation of the Hartmann number, the reference magnetic field (of the order of magnitude of 0.08 T) consisted of the axial component B_z at mid-height upon the cylinder wall, which was obtained through extrapolation of a curve analogous to that of Fig. 1. Examination of Fig. 2(b), drawn up for Re = 615, indicates that functions $\Delta P_{(\theta)}$, obtained when M = 0 (insulating cylinder and absence of a magnetic field of external origin) and M = 20 (permanent magnet), were of nearly the same shape and deducible, one from the other, by a weak translation along the ΔP axis. This translation is principally due to the presence of an electromagnetic pressure gradient inside the duct.

In summation, the boundary layer around a cylindrical permanent magnet is virtually unchanged by the magnetic field generated by itself and, for a given Reynolds number, remains identical to that of a cylinder of the same diameter in classical fluid mechanics [16]. It follows that the eddy currents which travel through the boundary layer are weak. Therefore, this finding, verified for $50 < Re < 15000$, is comparable to the findings already mentioned in the study of flows around non-magnetic, insulating and conducting cylinders in the presence of an axial magnetic field [11].

2.3. *Voltage and electric field*

The experimental magnet used was identical to that described in section 2.1. The obstacle was placed at the center of a square cross-section of an annular vessel (Fig. 3) of depth h = 8 cm, R_1 = 9 cm and R_2 = 14.5 cm radii, fabricated from Plexiglas, and containing mercury with a free surface. The vessel being moved with a constant angular velocity ω_0, a uniform flow was established and the velocity, at a point with coordinate r along a radial axis $\vec{Or}$, was given by $u = \omega_0 r$. A speed reduction gear permitted variations of u ranging from 1 to 300 mm s^{-1}.

Two antipodal electrodes (AA') with a distance between them of D = 5.95 mm were placed at mid-height on the magnetized cylinder. Two additional electrodes (aa'), separated by approx. 1 mm, were situated upon the circle of diameter D, symmetric with respect to the midperpendicular of AA' (Fig. 3). The obstacle was capable of rotating around its Δ revolution axis at an angle α as long as $\pi/2 > \alpha > -\pi/2$ (Fig. 3). Two electrode tips (BB') and a moving electrode C were fitted upon the plane AA'aa'. Potential differences V between the ends of the electrodes were drawn up by means of a nanovoltmeter (Keithley mod. 148).

Whatever the position of the points B and B', for a given velocity **u**, we checked by experiment the relations

$$V_{AA'} = V_{AB} + V_{BB'} + V_{B'A'}$$

and

$$V_{AA'} = \int_{AA'}^{dV_{aa'}} \text{(along a semicircle of diameter } D\text{)},$$

$$= \int_{\alpha=-\pi/2}^{\alpha=\pi/2} dV_{aa'}.$$

When we inserted into the flow a two-electrode potential-difference sensor [1, 6, 17], the tips e and e' being separated by a short distance dl of about 2 mm, the component of the electric field E in the direction of

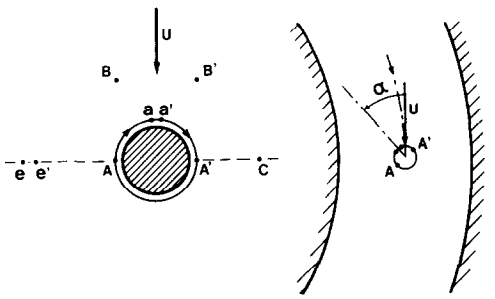

FIG. 3. Schematic diagram of the measurement devices for voltage, electric field and velocity.

dl could be defined at M, midpoint of ee', by

$$E_M = \frac{dV_{ee'}}{dl}.$$

By means of the two-electrode potential-difference sensor ee', or with the travelling electrode C (Fig. 3), we were able to measure the radial component of the electric field E along the $\overrightarrow{0r}$ axis from the point A (or A'). The component parallel to **u** was of zero value, and the axial component parallel to the Δ-axis was found to be negligible due to weak values of the radial component B_r of the magnetic field as mentioned previously in section 2.1. Thus the magnitude of the electric field E was almost equivalent to E_M. In Fig. 1, E is drawn up for a constant velocity **u**, showing that the electric field E_r is quite nearly equal to the ratio $(B_z(r))/u$ of the magnetic field's axial component to the upstream undisturbed value of the velocity u.
Accordingly, inside the flow

$$E \simeq u \cdot B.$$

Therefore E is practically the same as the vectorial product of **u** × **B** and, from Ohms law for moving media

$$\mathbf{J} = \sigma(\mathbf{E} + \mathbf{u} \times \mathbf{B})$$

it follows that

$$j \simeq 0.$$

This is a significant result. What is being shown, in effect, is that the electromagnetic force density **J** × **B** inside the liquid metal was negligible because the magnetic field generated by the permanent magnet decreased very rapidly along the $\overrightarrow{0r}$ axis (Fig. 1), meaning that the flow was almost completely undisturbed by a magnetohydrodynamic effect. An analogous finding was expressed earlier for the boundary layer (section 2.2.2).

Next we drew up the voltage $V_{AA'_M}$ corresponding to $\alpha = 0$ for different values of the velocity **u**. Systematic measurements allowed us to establish the relation

$$V_{AA'_M} = K \cdot B_z(D/2) \cdot u \cdot D$$

with

$$K = 0.94$$

hence

$$V_{AA'_M} = K_0 \cdot u.$$

In this experiment, electrodes A and A' were at a distance $d/10$ from the wall of the magnet of diameter d, thus placing them on the outside of the boundary layer which had a thickness of the order of magnitude of $d/20$ [16] for the range of the Reynolds number study ($200 < Re < 15000$).

The behaviour of this device was found to be similar to that of a two-electrode potential-difference sensor subjected to an external magnetic field of magnitude $B_z(D/2)$ identical with the field produced on the electrode tips AA' by the magnet, provided that the potential-difference sensor was placed on a point inside the flow where the fluid has a velocity of **u** and an electric current density **J** of zero value. In this case the voltage is proportional to the electromotive field **u** × $\mathbf{B}_z(D/2)$. Numerous tests conducted with magnets of different diameters and fabricated from materials of various ferromagnetic properties corroborated this finding. For an incidence α (Fig. 3), we can verify by experiment the simple relation

$$V_{AA'} = V_{AA'_M} \cos \alpha,$$

$V_{AA'_M}$ being the voltage when $\alpha = 0$.

3. DESCRIPTION OF THE PROBE

The probe shown in Fig. 4 was essentially made up of a cylindrical permanent magnet (m) and one or two pairs of antipodal electrodes (e) situated at the midheight of the magnet. A jacket (c) fastened to the probe-holder kept the magnet in place as well as the electrodes, which were electrically insulated (i) except at their end points. Selection of materials for fabrication of the probes depends above all else upon the working temperatures they were to be used at. For tests at room temperature, or not exceeding 200°C, 'Coramag' permanent magnets made from cobalt–rare-earth (samarium) were employed. These were found to have very high specific magnetic energy, an exceptional resistance to demagnetization in the presence of unlike magnetic fields, as well as the following features:

Residual magnetism	0.83 T,
Coercive force	650 kA m^{-1},
Product (BH) maximum	135 kJ m^{-3},
Temperature of change of structure	250°C,
Curie point	710°C.

Electrodes were made from copper (or platinum) wire core (0.2 mm dia.) and covered with an insulating varnish.

For high temperature testing, we used 'Alnico 600' metallic magnets with specially refined basic constituents of nickel, cobalt, aluminium and iron. These high residual magnetism and high specific magnetic energy magnets possess the property of retaining half magnetization at 700°C. In this case, the probe-holder

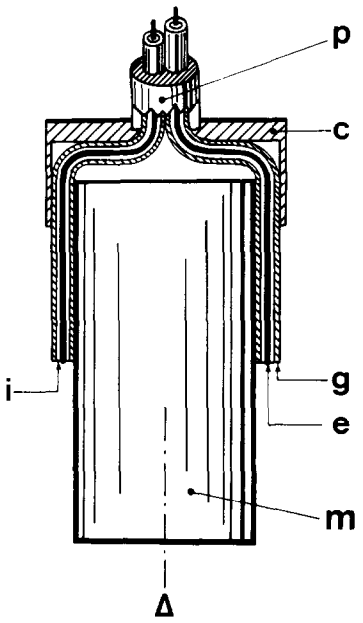

FIG. 4. Schematic diagram of the probe: (p) probe-holder, (c) jacket, (e) wire core, (g) conductor sheaths, (i) insulator, (m) permanent magnet, (Δ) revolution axis.

(p), the cylindrical jacket (c), the electrodes (e) and their sheaths (g) were fashioned from stainless steel (Fig. 4). Electric insulation (i) between electrodes and conductor sheaths was assured by highly compacted magnesia.

The features noted below correspond to 'Alnico 600' permanent magnets of ordinary (parallelepiped, cylinder) shape with volumes greater than 1 cm^3 and all dimensions greater than 0.8 cm.

Residual magnetism	1.26 T,
Coercive force	50 kA m^{-1},
Product (BH) maximum	42 kJ m^{-3},
Curie point	860°C.

4. BEHAVIOR AT ROOM TEMPERATURE

4.1. *Steady state*

The Δ revolution axis of the sensor and the directions AA′ and BB′ formed a trirectangular trihedron $0xyz$ (Fig. 5). In addition, the direction of the velocity of magnitude u was determined by the angles θ and ϕ with

$$|\mathbf{u}| \begin{cases} u_x = u \sin\phi \sin\theta, \\ u_y = u \sin\phi \cos\theta, \\ u_z = u \cos\phi. \end{cases} \quad (1)$$

The probe was again inserted into mercury held by the toroidal channel (section 2.3.) and a mechanical system permitted the reproduction of conditions in Fig. 5 and the setting of all θ and ϕ angles. A systematic study was then carried out by making the u, θ, ϕ parameters vary independently.

4.1.1. *Operation with normal incidence.* In the case where the vector **u** is perpendicular both to AA′ and Δ axis ($\theta = \phi = \pi/2$ and $u_x = u$), we found that regardless of the magnitude of u, results were the same as those presented in section 2.3

$$V_{AA'} = K_0 \cdot u, \quad V_{BB'} = 0$$

and

$$V_{AA'} = 0, \quad V_{BB'} = K_0 \cdot u$$

when

$$\theta = 0 \text{ and } \phi = \frac{\pi}{2} \quad (u_y = u).$$

For a Coramag magnet of diameter $d = 2$ mm and length $l = 3$ mm, the sensitivity is of the order of 2 μV per cm s^{-1}. When we used magnets with diameters greater than 2 mm, $B_z(D/2)$ increased and consequently the signal delivered by the sensor also increased. As an example, when $d = 3$ mm, the response was 4 μV per cm s^{-1} and the value of the axial components of the magnetic field $B_z(D/2)$ upon the electrode ends was approx. 0.14 T.

These measurements, made inside a mercury flow where the velocity is known in magnitude and direction, permit calibration of the probe at room temperature. The calibration factor K_0 depends on the constituents of the magnet, the dimensionless parameter

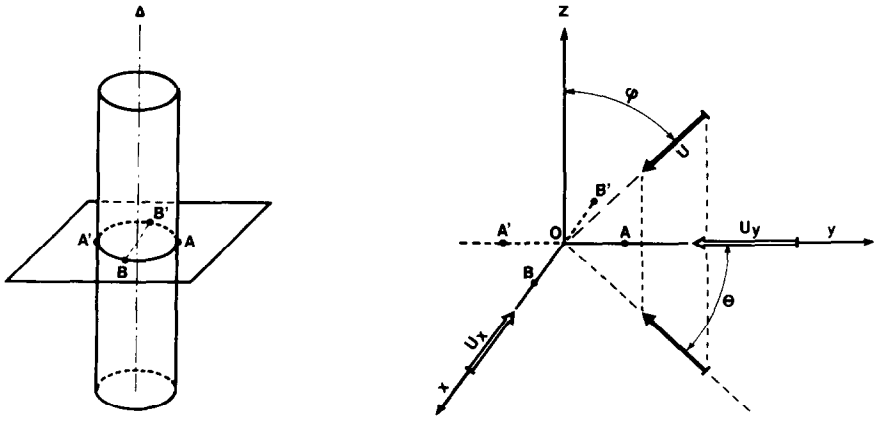

FIG. 5. Schematic of the determination of magnitude and direction of velocity in a 3-dim. flow.

d/l and the distance D between the electrodes. Occasionally this constant may be slightly different for the pairs AA′ and BB′ on account of a design defect in the perpendicularity between AA′ and BB′.

Due to the finite dimensions of the magnet, fringe phenomena occur where the fluid flows over the ends, i.e. into an area where the magnetic field is strongest and normal to the poles. Systematic experiments showed that as long as the ratio of d/l was less than one, the response of the probe as a function of the velocity remained linear. In addition, the factor calibration was again between 0.9 and 1. Best performances were obtained for a value of d/l equal to 0.66, corresponding approximately to a maximum strength of $B_z(D/2)$.

To verify results obtained by the first process, an incorporated magnet probe (S) and a Pitot–Prandtl tube (P) were used to plot successive velocity profiles at mid-depth of the rotating vessel downstream from a 3 mm dia. fixed cylindrical obstacle (Fig. 6a) and a widening (Fig. 6b). Examination of these profiles showed satisfactory agreement of results obtained by the two processes in cases where local velocity distributions were non-uniform.

4.1.2. *Operation with any incidence.* Giving at first the constant value $\pi/2$ to angle $\phi(u_z = 0)$, we experimentally verified the following relations:

$$V_{AA'} = K_0 u \sin\theta = K_0 u_x,$$

$$V_{BB'} = K_0 u \cos\theta = K_0 u_y.$$

In the general case of a tridimensional flow where the direction of **u** was unknown, we oriented, as a first step, the Δ axis of the probe in a parallel direction to $\vec{0z}$ (Fig. 5) and drew up the voltages

$$V_{AA'} = K_0 u \sin\phi \sin\theta = K_0 u_x,$$

$$V_{BB'} = K_0 u \sin\phi \cos\theta = K_0 u_y.$$

Afterwards, pointing the Δ axis in a parallel direction to $\vec{0y}$, we attained to the u_z component and again found u_x

$$V_{AA'} = K_0 u \sin\phi \sin\theta = K_0 u_x,$$

$$V_{BB'} = K_0 u \cos\phi \qquad = K_0 u_z.$$

It is also possible to orient the Δ axis in a direction parallel to $\vec{0x}$, which permits finding u_y and u_z again.

It is important to note that a previous marking of electrode connections with respect to the input terminals of the nanovoltmeter is essential because measured potential differences, being proportional to an electromotive field of the form $\mathbf{u} \times \mathbf{B}$ (section 2.3), change sign when the direction of the velocity components reverses.

In summary, the calibration factor being known, the measurement of two voltages $V_{AA'}$ and $V_{BB'}$, for two successive orientations of the revolution axis of the probe, yields three equations (1) allowing the determination of the direction (angle θ and ϕ) and the magnitude of the velocity $|\mathbf{u}| = (u_x^2 + u_y^2 + u_z^2)^{1/2}$.

Figure 7 presents an example of flow pattern

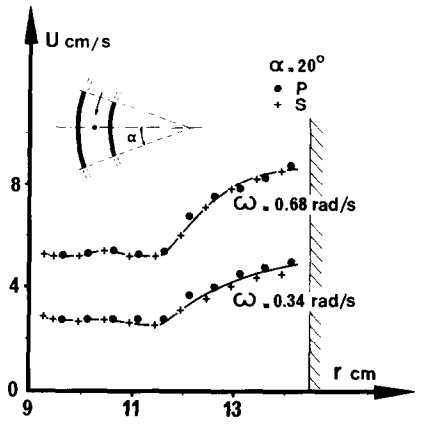

FIG. 6(a). Velocity distributions plotted by means of a Pitot tube (P) and an incorporated magnet probe (S) downstream from a small cylinder.

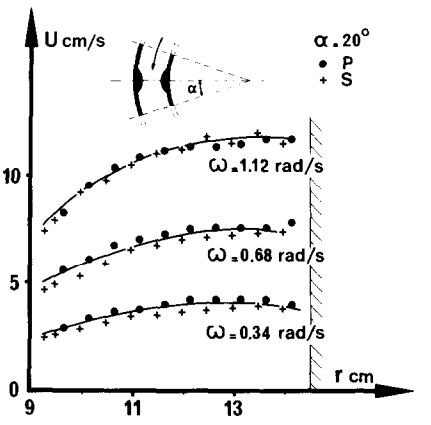

FIG. 6(b). Velocity distributions plotted by means of a Pitot tube (P) and an incorporated magnet probe (S) downstream from a widening.

plotting in a 2-dim. velocity field. The device consisted of a rectangular (15 × 45 mm) cross-section loop containing mercury and moving at the average velocity of U_x. The molten metal, held in a parallelepipedal cavity of dimensions 140 × 140 × 45 mm (Fig. 7), was driven by viscous effects. All walls were of Plexiglas 1 cm thick. Plexiglas is not a perfect insulating material, consequently the experiment was not rigorously isothermal. A slot made in the upper horizontal wall permitted the vertical and horizontal shifting of the probe upon the plane of symmetry, vertical and parallel to U_x, of the chamber. Plotting of the u_y and u_z components makes possible the determination of the magnitude and the direction of the velocity at every point. We observed, when $U_x = 5\,\mathrm{cm\,s^{-1}}$, a principal cell which nearly filled the entire cavity. A small recirculating vortex could also be detected in the upper left corner of the cavity. It is relatively easy to plot horizontal and vertical profiles of velocity components as well as to determine, after graphical integration, flow rates and mass transfer.

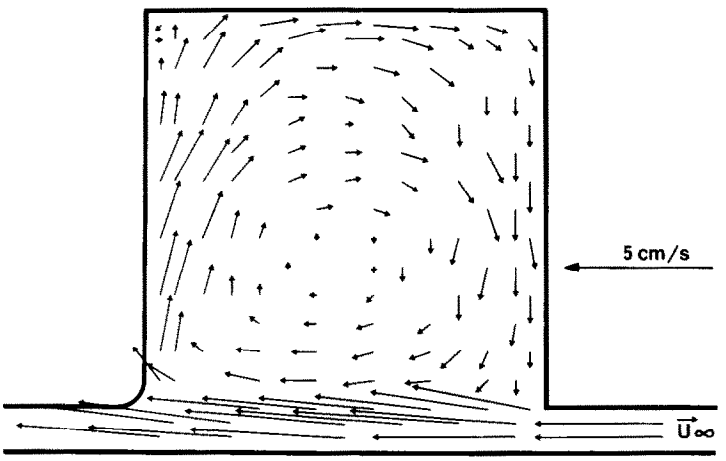

FIG. 7. Velocity measurements in the vertical plane of symmetry of a rectangular cavity (140 × 140 × 45 mm) situated above a mercury loop of cross section 45 × 15 mm.

4.2. *Unsteady state*

The sensor was placed at the center of a Plexiglas parallelepipedal tank (8 × 9 × 4 cm) filled with mercury (Fig. 8). A thin slot made in the upper horizontal wall of the vessel permitted the insertion of the probe which was fixed in the laboratory frame. The tank was driven with a sinusoïdal motion generated by a vibration exciter (Brüel and Kjaer type 4808) having a frequency range of 5 Hz–10 kHz and exerting a force rating of 112 N sine peak. The magnitude a, the angular velocity ω (or the frequency N) and thus the maximum velocity $U_m = a\omega$, may be modulated at will by means of the Brüel and Kjaer measuring chain presented in Fig. 8.

An accelerometer of delta shear design type 4370 fastened to the closed holder produced an electrical output proportional to the vibratory acceleration to which it was subjected. This response was transmitted to a vibration meter type 2514 that provided the RMS values of acceleration and velocity, as well as the peak-to-peak displacement values. Matching the high output impedance of the accelerometer and the input impedance of the measuring analysis instrumentation was made possible by a charge amplifier type 2634. Two type 2120 frequency analysers (band pass 0.1 Hz–300 kHz) permitted reaching the RMS values of the voltage $V_{AA'}$ and $V_{BB'}$ which were increased beforehand by measuring amplifiers, type 2610, of 10^4 gain (band pass 2 Hz–20 kHz). Finally a type 2971 phasemeter was used to measure the phase angle between the voltage produced by the accelerometer (in phase with the acceleration of the liquid metal) and $V_{AA'}$ (or $V_{BB'}$).

In another set of experiments, the tank was held motionless in the laboratory frame while the probe was driven with a sinusoidal motion; we found that for the same value of the relative maximal velocity U_m between the probe and the fluid, identical results were obtained.

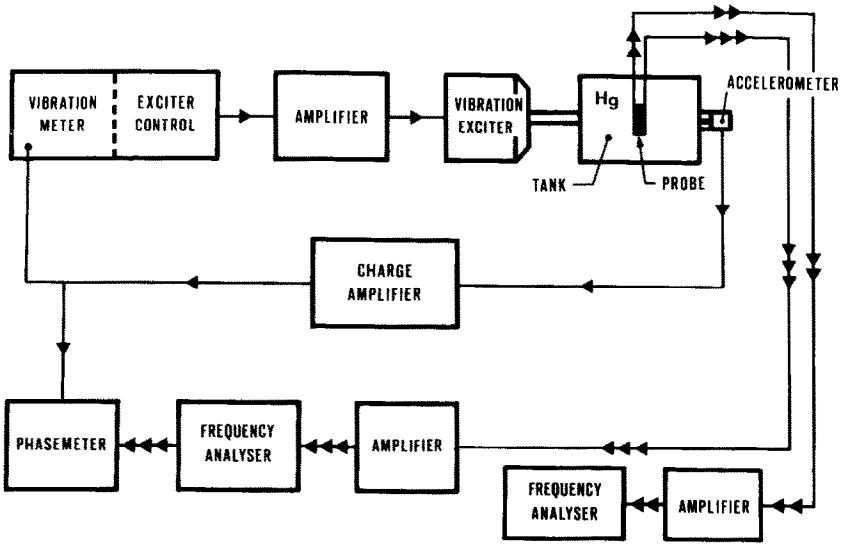

FIG. 8. Measuring chain in unsteady state.

Systematic measurements made it evident that the response of the sensor is proportional to the RMS value U' of the velocity of the fluid and separately independent from the frequency N and the magnitude a of motion. Furthermore, no phase difference was perceived between the instantaneous velocity and the responses given by the coupled electrodes AA' and BB'. Experimental runs established that, in the frequency range studied ($0 < N < 50$ Hz), the sensor responded instantaneously and, even more important, the calibration it provided in steady flow holds true in unsteady flow for the RMS of the local velocity. Therefore the probe is suitable to the measurement of local velocities inside time varying flows such as those characterized by transient or alternating motion. A note of warning must be sounded, however, because due to the sizes of the sensors ($d = 2$ mm and $l = 3$ mm for the smallest) the use of this technique in the study of random phenomena (instabilities and turbulence) should be considered with prudence, except in the case of large vortices.

5. BEHAVIOUR AT HIGH TEMPERATURE

In this study, we again used an annular vessel fabricated from stainless steel with a 1 cm thickness, depth $h = 8$ cm, $R_1 = 4$ cm and $R_2 = 13$ cm radii. The metal was kept in a melted state by two propane burners, with temperature control provided by means of an immersion pyrometer. The entire device was surrounded by four vertical walls of refractory materials (Siporex). The sensors tested were 'Alnico 600' magnets (section 3) with diameter d ranging between 4 and 8 mm and height h between 8 and 12 mm. Tests consisted of systematically drawing up voltage values $V_{AA'}$ within various molten metals for velocity values ($0 < u < 30$ cm s^{-1}) and temperature values (18°C $< T <$ 760°C) and when $\theta = \pi/2$.

The results shown in Fig. 9 demonstrate that the response of the probe, as a function of the velocity and for a constant temperature, is always linear and is independent of the type of molten metal (lead, tin, zinc). Moreover, the factor $K_{(T)}$ of the relations

$$V_{AA'} = K_{(T)}u$$

decreases as the temperature increases.

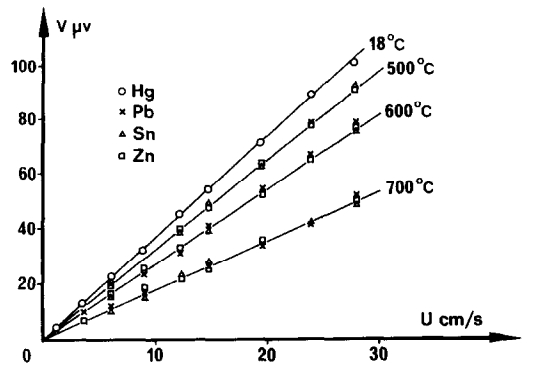

FIG. 9. Calibration of the probe for different temperatures.

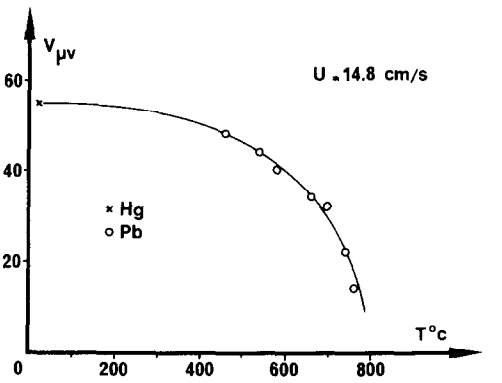

FIG. 10. Response of the probe as a function of temperature for a constant velocity.

Figure 10 presents, for a constant velocity, the variations of $V_{AA'}$ as a function of the temperature. In this experiment the working fluid was molten lead. When several cycles between 450°C and 760°C were traced (temperature rise or descent time being between 1 and 2 h) we found a reversible phenomenon in that the same response was found again by coming back to a given initial temperature. Furthermore, tests carried out during a 10 h period, at constant temperature and velocity, revealed that the response of the sensor remained virtually unchanged, establishing that the ageing of the Alnico magnet does not take place in these conditions. Experiments on molten zinc, however, revealed that a 4 h time limit must not be exceeded due to corrosion of the stainless steel electrodes, followed by their rapid dissolution.

Thus we verified that

$$V_{AA'} = K \cdot B_z(T) \cdot u \cdot d$$

$$= K_{(T)} \cdot u$$

and the factor $K_{(T)}$, which varies as the function $B_z(T)$, follows the magnetization variations of the permanent magnet as a function of temperature, and as is well known, the decreasing of $B_{(T)}$, though starting slowly at room temperature, becomes very rapid in the vicinity of the Curie point. We also perceived that the signal is no more than 0.96 V_r at 300°C, 0.73 V_r at 600°C, and 0.55 V_r at 700°C, from a reference response V_r chosen for a given velocity at 18°C.

The fundamental study carried out here established that voltage $V_{AA'}$ was due uniquely to the integration of the electric field **E** along an open path, this electric field being nearly equal and opposed to the electromotive field $\mathbf{u} \times \mathbf{B}$. Therefore it is obvious, on account of the absence of a magnetohydrodynamic effect in both the boundary layer and the current flow, that the signal is independent of the kind of fluid. The function $K_{(T)}$ being identical for all molten metals, it is only a matter of first carrying out an easy calibration at room temperature (with mercury) and then adapting this calibration to higher temperatures with the magnetization variation curve of the magnetic material (Alnico 600) as a function of the temperature (Fig. 10).

Table 1

	$(kg\,m^{-2})$	$(m^2\,s^{-1})$	$(\sigma \times 10^6\,mho\,m^{-1})$	Re	M	N
Mercury	13550	1.15×10^{-7}	1.05	5200	6	0.007
Tin	6957	2.53×10^{-7}	2.05	2370	8.2	0.028
Zinc	6919	4.61×10^{-7}	2.83	1300	7.15	0.039
Lead	10510	2.01×10^{-7}	1.08	2990	5.45	0.010
Aluminium	2380	1.22×10^{-6}	5.1	490	9.65	0.19
Sodium	927	7.6×10^{-7}	10.4	790	17	0.37

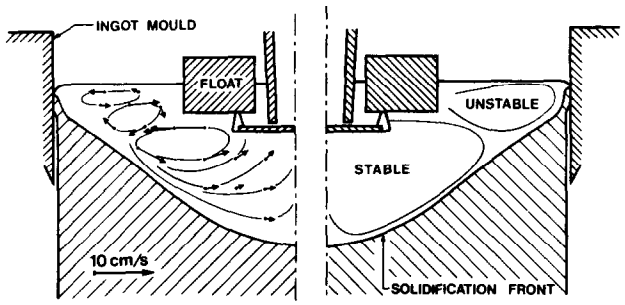

FIG. 11. Velocity measurements in continuous casting in the sump of an aluminium alloy 7049 billet with a 320 mm dia.

Table 1 presents the mechanical and electrical parameter values of the experimental metals (at 20°C for mercury and melting point for the rest). The Reynolds, Hartmann and Stuart numbers were calculated from the diameter d of the magnet when $d = 0.6$ cm, $u = 10\,cm\,s^{-1}$ and $B_z = 0.04\,T$.

Examination of this table shows weak values for the Hartmann number and the interaction parameter, which brings in further reasons to neglect effects having magnetohydrodynamic origins.

Certain practical comments with regard to sensor use at higher temperatures are necessary at this point. It is of primary importance at the insertion of the probe into the molten metal to scatter the oxide film, which covers the free liquid surface and can cause poor electrical contact between the liquid and the electrode tips. In addition, we found it indispensible when measuring weak velocities of the order of $1\,cm\,s^{-1}$ to cancel a stray voltage of about $1\,\mu V$ which remained from the thermal shock at the insertion of the probe. For that, we set the nanovoltmeter back to zero after immersing the probe in a spoonful of the molten metal nearly at rest.

In metallurgy, the nature of mass transfer in the vicinity of the solidification front is known to have a primary effect on the motion of nuclear crystals and crystal growth, on the possible development of dendrites, the homogeneity and the volume of the grain, and consequently, on the mechanical properties of the metal [18]. However, until the formulation of suitable sensors, these flows have remained poorly understood and largely beyond our ability to explore them.

Figure 11 presents an illustration of local velocities taken in a temperature range from 630 to 670°C inside the sump of a 320 mm dia. billet of aluminium alloy 7049, which was produced in continuous casting with a lowering rate of $60\,mm\,min^{-1}$. In this experiment, a thermocouple of 0.25 mm dia. was fastened to the probe. Figure 11 reveals the presence of two main cells (and of a recirculating vortex inside the upper left zone). The existence of these two cells is explained by a viscous friction phenomenon caused by the radial and horizontal pouring jet running out of the float (analogous to effects presented in Fig. 7). The recording of signals emitted by the sensor allowed, on account of the sensor's instantaneous response time, the boundary mapping of a rather unstable zone where fluctuations of velocity were 30% greater than average values, and of a stable lower zone where velocities did not exceed $1\,cm\,s^{-1}$.

6. CONCLUSIONS

In the absence of a magnetic field of external origin, the probe presented has allowed, by a simple voltage measurement, the determination of local velocities in molten metals within the range $0–10\,m\,s^{-1}$ with a sensitivity of $1\,mm\,s^{-1}$. This technique is applicable in metal baths with temperatures as high as 720°C and has a field of application including mercury, tin, zinc, aluminium and sodium, as well as their numerous alloys.

Due to responses that are steady, instantaneous, and proportional to the velocity of the liquid metal, these sensors are particularly adapted to the automatization and regulation of continuous, semi-continuous and pulsating castings.

This probe, because it has the property of finding locally the magnitude and direction of velocity, allows for the first time the study of mass transfer in the heat

exchange of nuclear reactors using alkaline metals as coolant fluids. It also makes possible the plotting of velocity distribution within molten metal flows as encountered in metallurgy. Last of all, in the case of large vortices, the possibility of turbulence study is offered.

REFERENCES

1. H. Branover, *Magnetohydrodynamic Flow in Ducts*. John Wiley (1978).
2. M. Sajben, Hot wire anemometer in liquid mercury, *Rev. Scient. Instrum.* **36**, 945–949, 1965.
3. J. C. Hill and C. A. Sleicher, Directional sensitivity of hot-film sensors in liquid metals, *Rev. Scient. Instrum.* **42**, 1461–1468 (1971).
4. D. G. Malcolm, Some aspects of turbulence measurement in liquid mercury using cylindrical quartz-visulated hot-film sensors, *J. Fluid. Mech.* **37**, 701–714 (1969).
5. M. Hoff, Hot-film anemometry in liquid mercury, *Instrums Control Syst.* **42**, 83–86 (1969).
6. I. A. Platnieks, Comparison of the hot wire anemometer and conductions methods for mercury measurements, *Magnit. Gidrod.* **7**, 140–142 (1971).
7. P. S. Lykoudis and P. F. Dunn, Magneto-fluid-mechanics heat transfer from hot-film probe, *Int. J. Heat Mass Transfer* **16**, 1439–1452 (1973).
8. R. J. Holroyd, Hot-film probe velocity measurements in liquid metal, M.H.D. duct flow experiment, *DISA Inform.* **25**, 19–24 (1980).
9. Ch. Vives, R. Ricou and A. Chambarel, Procédés et dispositifs pour mesurer localement des vitesses instantanées d'un fluid électroconducteur, notamment d'un métal fondu, French patent, ANVAR no. 79/19 818 (1979).
10. J. B. Kolesnikov, A. B. Cinober and E. V. Shcherbinin, Experimental study of the magnetohydrodynamic drag of a cylinder, *Magnit. Gidrod* **2**, 45–48 (1968).
11. Ch. Vives, Sur le coefficient de traînée de pressions d'un obstacle cylindrique en magnetodynamique des liquides, *C.r. hebd. Séanc. Acad. Sci., Paris* **278B**, 501–504 (1974).
12. Ch. Vives, Etude d'écoulements autour d'obstacles cylindriques isolants et électroconducteurs en présence d'un champ magnétique transversal, *C.r. hebd. Séanc. Acad. Sci., Paris* **280B**, 677–680 (1975).
13. Ch. Vives, Sur le coefficient de traînée de pressions des cylindres ferromagnétiques en magnétodynamique des liquides, *C.r. hebd. Séanc. Acad. Sci., Paris* **288B**, 233–236 (1979).
14. S. Globe, The effect of a longitudinal magnetic field on pipe flow of mercury, *Trans. Am. Soc. Mech. Engrs*, Series C, *J. Heat Transfer* **4**, 445–453 (1961).
15. L. G. Kit, D. Peterson, I. A. Platnieks and A. B. Tsinober, A study of the influence of fringe effects on M.H.D. flow in a channel with nonconducting walls, *Magnit. Gidrod.* **4**, 47–53 (1970).
16. S. F. Hoerner, *Resistance à l'Avancement dans les Fluides*. Gauthier-Villars, Paris (1965).
17. J. A. Shercliff, *The Theory of Electromagnetic Flow Measurement*. Cambridge University Press (1962).
18. D. B. Spalding and N. H. Afgan, *Heat and Mass Transfer in Metallurgical Systems*. McGraw-Hill (1981).

DETERMINATION DES VITESSES LOCALES ET DES TRANSFERTS DE MASSE DANS LES METAUX FONDUS AVEC LA SONDE A AIMANT INCORPORE

Résumé—On décrit une sonde permettant de déterminer le module et la direction de la vitesse, en tout point, pour des régimes stationnaires ou variables dans le temps, an sein d'un métal fondu. L'interprétation du principe de fonctionnement de cette sonde est fondé sur une étude expérimentale relative á l'écoulement d'un métal liquide autour d'un aimant cylindrique. Il est possible de mesurer des vitesses locales comprises entre 0 et 10 m s^{-1}, avec une sensibilité de l'ordre du mm s^{-1}, dans des bains dont la température peut atteindre 720°C. Des exemples de distribution de vitesses, relevées à la température ordinaire (mercure) et á 670°C (alliages d'aluminium), dans des écoulements comportant des tourbillons sont présentés.

BESTIMMUNG DER LOKALRICHTUNGEN UND DER MASSFÖRDERUNGEN IN FLÜSSIGMETALLEN DURCH EINE SONDE, IN DER EIN MAGNET EINGESTELLT IST

Zusammenfassung—Es handelt sich um die Beschreibung einer Sonde, durch die man in stationären, oder zeitlich veränderlichen Strömungen die Amplitude und die Richtung der Geschwindigkeit in allen Stücken einer Schmelze bestimmen kann. Es ist möglich, mit einer Empfindlichkeit von einem mm s^{-1}, in einem bis zum 720°C warmen Schmelzbad, von 0 bis zum 10 mm s^{-1} locale Geschwindigkeiten zu messen. Die Auswertung des Arbeitenprinzips dieser Sonde beruht auf Versuchsstudien des Fliehens eines Flüssigmetalls um einen zylinderförmigen Magnet herum. Es werden Beispiele von an der Raumtemperatur (Quecksilber) und an 670°C. Temperatur (Aluminiumlegierung) aufgenommener Geschwindigkeitenverteilungen in Wirbelfliehen vorgeführt.

ИЗМЕРЕНИЯ ЛОКАЛЬНОЙ СКОРОСТИ И МАССОПЕРЕНОСА В РАСПЛАВЛЕННЫХ МЕТАЛЛАХ МАГНИТНЫМ ДАТЧИКОМ

Аннотация—Описан датчик, позволяющий определять величину и направление скорости в каждой точке внутри объема расплавленного металла для стационарных или нестационарных условий. Принцип работы датчика разработан на основе экспериментального исследования обтекания жидким металлом цилиндрического магнита. В качестве примеров приведены распределения скорости в диапазоне температур от комнатной (ртуть) до 670°C (сплавы алюминия) в завихренных потоках. Результаты показывают, что локальные значения скорости в диапазоне от 0 до 10 м $сек^{-1}$ при чувствительности датчика порядка одного мм $сек^{-1}$ можно измерять в объемах вплоть до температур порядка 720°C.